

Studying wave optics in the light curves of exoplanet microlensing

Ahmad Mehrabi¹ and Sohrab Rahvar^{1,2} *

¹ *Department of Physics, Sharif University of Technology, P.O.Box 11365–9161, Tehran, Iran*

² *Perimeter Institute for Theoretical Physics, 31 Caroline Street North, Waterloo, Ontario N2L 2Y5, Canada*

7 November 2018

ABSTRACT

We study the wave optics features of gravitational microlensing by a binary lens composed of a planet and a parent star. In this system, the source star near the caustic line produces a pair of images in which they can play the role of secondary sources for the observer. This optical system is similar to the Young double-slit experiment. The coherent wave fronts from a source on the lens plane can form diffraction pattern on the observer plane. This diffraction pattern has two modes from the close- and wide-pair images. From the observational point of view, we study the possibility of detecting this effect through the Square Kilometer Array (SKA) project in the resonance and high magnification channels of binary lensing. While the red giant sources do not seem satisfy the spatial coherency condition, during the caustic crossing, a small part of source traversing the caustic line can produce coherent pair images. Observations of wave optics effect in the longer wavelengths accompanied by optical observations of a microlensing event provide extra information from the parameter space of the planet. These observations can provide a new basis for study of exoplanets.

1 INTRODUCTION

Gravitational lensing is caused by the bending of light rays due to the gravitational effect of a foreground mass. Depending on the distribution of mass on the lens plane and on the relative distances of the lens and source from the observer, multiple images or distortion in the source shape can be formed. In the case of star-star lensing inside the Milky Way, the separation between images is less than few milliarcseconds and the images are unresolvable for the ground based telescopes. This type of gravitational lensing is termed gravitational microlensing.

Einstein (1936) derived the gravitational lensing equation, but it was decades until the first gravitational lensing was observed in 1979. The source of this lensing was a quasar and observations were performed in radio frequencies (Walsh et al 1979). A few years later Paczyński proposed studying the MACHO (Massive Astrophysical Compact Halo Objects) population in the Galactic halo by the method of gravitational microlensing (Paczynski 1986). His suggestion was to observe stars in the Large and Small Magellanic Clouds, counting the number of microlensing events and measuring their transit times (Einstein crossing time). Based on this observation one can measure the contribution of MACHOs to the mass of Galactic halo. In addition to dark matter studies, another interesting astrophysical application of microlensing was suggested by Moa & Paczynski (1991), namely the use of gravitational microlensing to aid in the discovery of exoplanets.

Microlensing effect due to single or multiple lenses have been studied mainly using geometric optics. An important study of wave optics features of gravitational lensing was undertaken by Ohanian (1983), who investigated the magnification of a radio point source when a galaxy acts as a gravitational lens. He showed that wave optics smoothes singular features of the light curve at the position of caustic lines. In another work, Jaroszyński and Paczyński (1995) stud-

ied the caustic crossing of Quasar Q2237+0305 by a galaxy composed of individual stars. By studying the diffraction images of this system, they could put limit on the size of the quasar. Wave optics observation of gravitational lensing inside the Milky Way also have astrophysical applications, for example studying the limb darkening of small sources like white dwarfs (Zabel & Peterson 2003). Recently, Heyl (2010,2011a,2011b) discussed the possibility of detecting wave optics signals in microlensing light curves with a single substellar lens.

In this work our aim is to extend the application of the wave optics to the conventional method of extra solar planet detection by gravitational microlensing. Here we assume a binary lens composed of a lensing star and a planet. The crossing of the caustic lines of this system by the source star produces high magnification in the light curve. Moreover, owing to the small separation of the images on the lens plane, the gravitational lensing system resembles a multiple slit optical system in the astronomical scales. With a coherent condition for the wave fronts on the lens plane, the result would be a diffraction pattern on the observer plane. We study the applications of this method in both the resonance and high magnification channels of the exoplanet detection. Observations of the contrast in the fringes and transit time of the fringes enable us to break degeneracy between the lens parameters. We also study the possibility of observing the wave optics features of binary microlensing using the future Square Kilometer Array (SKA) project.

In section 2, we introduce wave optics formalism in gravitational lensing and calculate the wave optics light curve for a binary lens system. In section 3 we carry out semi-analytic calculations of the wave optics feature for microlensing near the caustic lines and study the temporal and spatial coherency conditions. We also numerically compute wave optics light curves and compare them with the results of geometric optics. In section 4 we discuss the possibil-

ity of detecting microlensing wave optics signals by a binary lens in which one of the lenses is a planet. Our study uses observation in radio or micrometer wavelengths and future observations with SKA. We also discuss possibility of degeneracy breaking between the lens parameters in the resonance and high-magnification channels of exoplanet detection. Conclusion and a summary are given in section 5.

2 WAVE OPTICS IN GRAVITATIONAL LENSING

In geometrical optics, the locations of the images in terms of position of the source can be obtained from the lens equation

$$\mathbf{y} = \mathbf{x} - \alpha(\mathbf{x}), \quad (1)$$

where \mathbf{x} and \mathbf{y} are respectively the angular positions of the image and source normalized to the projected Einstein angle in each plane and $\alpha(x)$ is the deflection angle, which depends on the distribution of matter as

$$\alpha(\mathbf{x}) = \frac{1}{\pi} \int \kappa(\mathbf{x}') \frac{\mathbf{x} - \mathbf{x}'}{|\mathbf{x} - \mathbf{x}'|^2} d^2 x', \quad (2)$$

where $\kappa(x) = \Sigma(x)/\Sigma_{cr}$, $\Sigma(x)$ is the surface mass density of the lens, and $\Sigma_{cr}^{-1} = (4\pi G D_d D_{ds})/(c^2 D_s)$. Here, D_s , D_{ds} , D_d are the source-observer, lens-source and lens-observer distances, respectively. Another method for deriving lens equation is to use the Fermat principle. For the stationary points of the Fermat potential, the position of images in terms of the position of source is obtained from

$$\nabla_{\mathbf{x}} \phi(\mathbf{x}, \mathbf{y}) = 0, \quad (3)$$

where Fermat's potential is given by

$$\phi(\mathbf{x}, \mathbf{y}) = \frac{1}{2}(\mathbf{y} - \mathbf{x})^2 - \psi(\mathbf{x}), \quad (4)$$

and the deflection angle is

$$\alpha(\mathbf{x}) = \nabla_{\mathbf{x}} \psi(\mathbf{x}). \quad (5)$$

We use the determinant of Jacobian of the mapping function from the source plane to the lens plane. The magnification of a point-like source can be obtained as

$$\mu(x_i) = \frac{1}{|\det J(x_i)|} = \frac{1}{|\phi_{11}(x_i)\phi_{22}(x_i) - \phi_{12}^2(x_i)|}, \quad (6)$$

where x_i is the location of the i th image. For an extended source, we should calculate the magnification over the source area. One of the methods of calculating the magnification by an extended source is Green's theorem. In this theorem, a two-dimensional integration over the source reduces to a one-dimensional integration on the boundary of the images (Dominik 2007).

From the Huygens principle in wave optics, every point on the lens plane can be considered as a secondary source. The amplitude of the electromagnetic wave at each point of the observer plane is composed of the superposition of the infinitesimal sources on the lens plane. From the Kirchhoff integral, we can obtain the amplitude of the electromagnetic wave $F_{\mu\nu}$ if we know the boundary condition on the lens plane (Born and Wolf 2002). Multiplying the superposition of the electromagnetic wave by its complex conjugate results in the magnification of the wave on the observer plane as follows (Schneider et al. 1992):

$$\mu(\mathbf{y}) = \frac{f^2}{4\pi^2} \left| \int e^{if\phi(\mathbf{x}, \mathbf{y})} d^2 x \right|^2, \quad (7)$$

where $f\phi(\mathbf{x}, \mathbf{y})$ corresponds to the phase of the electromagnetic waves emitted from a source, deflected from the lens plane and received by the observer. Here f is given by $f = 2kR_s$ where k is the wave number and $R_s = 2GM_d/c^2$ is the Schwarzschild radius of the lens. This formula have been obtained for a monochromatic electromagnetic wave.

In order to show the compatibility of the wave optics formalism with that of geometric optics and the transition from the wave optics to the geometric optics formalism, we expand the Fermat potential in the lens plane using a Taylor series. For a point like source, the expansion around the image is given by

$$\begin{aligned} \phi(\mathbf{x}, \mathbf{y}) &= \phi^{(0)} + (\mathbf{x} - \mathbf{x}_i) \cdot \nabla_{\mathbf{x}} \phi^{(0)} + \frac{1}{2}[(x_1 - x_{1i})^2 \phi_{11}^{(0)} \\ &+ (x_2 - x_{2i})^2 \phi_{22}^{(0)} + 2(x_1 - x_{1i})(x_2 - x_{2i}) \phi_{21}^{(0)}] + \dots, \end{aligned} \quad (8)$$

where the superscript (0) represents the Fermat potential at the position of the image and subscripts represent the derivatives with respect to two directions on the lens plane. Substitute from equation (8) into (7), the first term of eq.(8) after multiplication of $\exp[i\phi(\mathbf{x}_i, \mathbf{y}_i)]$ by its complex conjugate results in unity. The second term is zero from the Fermat principle, and finally the third term as non-zero term results in the magnification in the geometric optics as equation (6). The third and higher orders of derivatives in the Fermat potential result in the wave optics features in the light curve.

One of the important issues in the wave optics formalism is that, in reality, the source is not completely coherent and we need to define a coherent time scale of $\Delta\tau = \Delta\omega^{-1}$, where $\Delta\omega$ is the width of the spectrum. The amplitude of a non-chromatic source on the observer plane is given by

$$V(\mathbf{x}, \mathbf{y}, \phi) \propto \int g(\omega) e^{i2R_s\phi(\mathbf{x}, \mathbf{y})\omega} d\omega,$$

where the magnification is given by

$$\mu(\mathbf{y}) = \frac{R_s^2}{\pi^2} \left| \int d^2 x \int g(\omega) e^{2iR_s\phi(\mathbf{x}, \mathbf{y})\omega} \omega d\omega \right|^2. \quad (9)$$

we set the speed of light to $c = 1$. For a coherent monochromatic source $g(\omega) = \delta(\omega - \omega_0)$ when substituting this specific spectrum in equation (9), we can recover equation (7). Assuming a non-zero temperature for a monochromatic source, the Doppler broadening can change the spectrum of a Dirac-delta spectrum to a Gaussian distribution.

An important issue regarding the observability of the wave optics effect is the coherency of light arriving to the observer from different parts of the lens plane, the so-called temporal coherency (Mandzhos 1981). In addition we need to have coherency between different parts of an extended source, termed spatial coherency. Assuming that a source has zero angular size, in order to examine the temporal coherency between different images, we need the time delay between the light rays from the source to the observer and compare it with the coherent time of the source. The time difference between the two light rays received by the observer is given by

$$\Delta t = 2R_s [\phi(\mathbf{x}_{I1}, \mathbf{y}) - \phi(\mathbf{x}_{I2}, \mathbf{y})], \quad (10)$$

where the source position is fixed and \mathbf{x}_{I1} and \mathbf{x}_{I2} are the positions of the images. The difference between the Fermat potentials, $\Delta\phi$, for two distant images is of the order of unity. On the other hand, during the caustic crossing, two pairs of close images can be formed with $\Delta\phi$ of the order of 10^{-3} . Quantifying the time delay for the

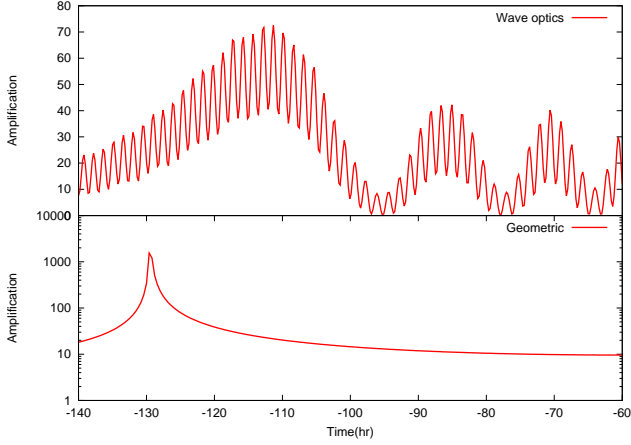


Figure 1. The wave optics light curve of a point like coherent source (upper panel) with the parameters of $d = 0.8$, $q = 0.1$, $u_0 = 0$, $t_E = 20$ days and $f = 1000$. Lower panel shows the light curve in the geometric optics. The light curves depict magnification of the source star during the caustic crossing.

wide and close pair of images in the caustic crossing, Δt is given as

$$\Delta t \sim 1 \times 2R_s \sim 10^{-5} \frac{M}{M_\odot} \text{ sec}, \quad \text{wide images} \quad (11)$$

and

$$\Delta t \sim 0.001 \times 2R_s \sim 10^{-8} \frac{M}{M_\odot} \text{ sec} \quad \text{close images}, \quad (12)$$

where in the former case images appear around the star-lens and in the latter case images appear around the planet-lens. Here we take the mass ratio of the planet to the parent star to be of the order of 10^{-3} . We will discuss this in detail in section (3). As the source approaches the caustic line (i.e. $\Delta t \rightarrow 0$), the time difference between the light rays become shorter. For a source with a non-zero temperature T_s , the coherent time in terms of the bandwidth of the spectrum is given by $\tau_c \Delta\omega \sim 1$ (Mehta 1963). The dispersion velocity of the gas is related to the surface temperature of a star by $\sigma \sim \sqrt{T_s}$, on the other hand, the dispersion velocity is related to the frequency dispersion as $\sigma = \Delta\omega/\omega$, hence the coherent time relates to the temperature of the source as (Guenther 1990):

$$\tau_c \propto \frac{1}{\sqrt{T_s} \nu} \Rightarrow \tau_c = \frac{2.8 \times 10^{-4}}{\nu(\text{GHz})} \sqrt{\frac{3000}{T_s}}. \quad (13)$$

In the double-slit experiment with a point-like source for a diffraction pattern, the time-difference between the two light rays received by the observer should not be longer than the coherent time. Now we can constrain $f = 2kR_s$ with a temporal coherency condition for the wide and close pair of images. Comparing equations (11) and (12) with the coherent time in equation (13) results in

$$f_{\text{wide}} \leq 10^6 \sqrt{\frac{3000}{T_s}}, \quad (14)$$

$$f_{\text{close}} \leq 10^9 \sqrt{\frac{3000}{T_s}}. \quad (15)$$

More details of temporal coherency in the wave optics gravitational lensing are given in Appendix (A).

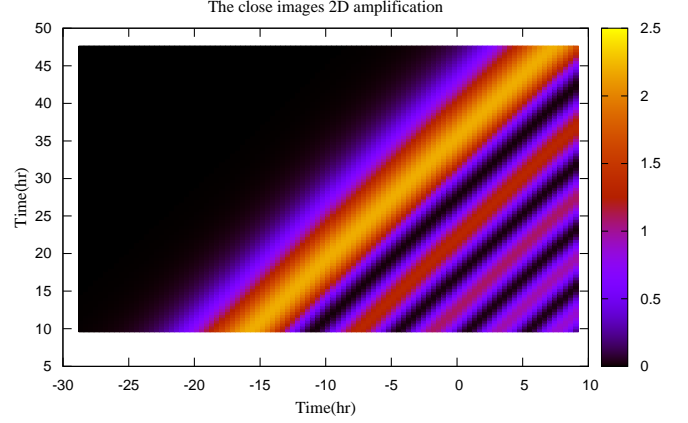


Figure 2. The two dimensional luminosity pattern from a point-like source on the observer plane lensed by a binary system. The fringes are demonstrated near a critical line. The overall flux results from the sum of the close images (as shown in this figure) plus flux from the incoherent wide images.

In order to calculate magnification by a binary lens composed of a parent star and a planet, we apply the following Fermat potential for a binary lens in equation (7),

$$\phi(\mathbf{x}, \mathbf{y}) = \frac{1}{2}(\mathbf{x} - \mathbf{y})^2 - m_* \ln(|\mathbf{x} - \mathbf{x}_*|) - m_p \ln(|\mathbf{x} - \mathbf{x}_p|), \quad (16)$$

where m_* and m_p are the relative mass of the star and planet to the overall mass of the system, respectively. The positions of the parent star and planet are given by \mathbf{x}_* and \mathbf{x}_p . We take lenses along the x_1 axis and put the center of mass of this system at $\mathbf{x} = 0$. The positions of parent star and planet are given by

$$\mathbf{x}_* = \left(\frac{d}{1+q}, 0 \right), \quad \mathbf{x}_p = \left(-\frac{d}{1+q}, 0 \right), \quad (17)$$

where d is the projected distance between the two lenses and it has been normalized to the Einstein radius and $q = m_p/m_*$. We can identify the track of the source on the lens plane by two parameters: the minimum impact parameter u_0 with respect to the center of mass of lenses and its direction with respect to x-axis, α . For the case of a single lens, the integral in equation (7) has an analytical solution; for two point-mass lenses, however, we perform numerical computations to obtain the light curve of a source moving with respect to the lens plane. In the next section, we utilize the Fourier expansion of the Fermat potential up to relevant terms, and study the Fermat potential of a binary lens near the caustic lines.

For a point-like source lensed by a binary system, we use equation (7) and plot the amplification pattern as a function of time in Fig. (1). This is a typical microlensing light curve with the wave optics features compared with those of geometric optics. Here we have two oscillating modes due to the interference between the wide and close images. As the source gets closer to the caustic line, the longer mode is magnified and after caustic crossing it becomes dimmer. In Fig. (2) we depict the two-dimensional pattern of fringes on the observer plane when the relative motion of the observer with respect to this pattern produces the light curve in Fig. (1). In the following section, we include the finite-size effect of the source star in our calculations.

2.1 Finite size effect

The majority of microlensing observations in recent years have been carried out by two MOA (Microlensing Observation in Astrophysics) and OGLE (Optical Gravitational Lensing Experiment observational groups, monitoring millions of stars toward the Galactic Center. There are other follow-up telescopes around the world that cover ongoing events for 24 h. These telescopes with high-cadence observations identify anomalies in the microlensing light curves to discover extra-solar planets. While there are all type of stars as microlensing targets towards the Galactic bulge, there is a selection bias for the red giant population compare to the main sequence stars (Moniez et al. 2012; Rahal et al. 2009). In the direction of Galactic bulge, red clump stars contain the majority of the source stars used for microlensing events (Hamadache et al 2006). This selection of source for the microlensing events is due to the brightness of red giants, which enable us to observe them from a distance. Consequently, the averaged Einstein angle corresponds to this type of source stars is larger than that for main sequence stars, making the transit time of these events longer. In addition to the visual band, red giants can optically pump interstellar medium and produce Maser emissions a few astronomical units away from the source star (Messineo et al. 2005; Vlemmings et al. 2005).

In contrast to the simple point-like sources, red giants are extended objects in which, extended source effect, not only decreases the strength of the magnification for geometric optics, but also decreases the enhancements of the fringes for wave optics (Schneider & Schmid-Burgk 1985). The overall magnification for an extended source is given by (Schneider et al. 1992)

$$\mu = \frac{\int_S \mu(\mathbf{y}) d^2\mathbf{y}}{\pi \rho^2}, \quad (18)$$

where $\mu(\mathbf{y})$ is the magnification of the multiple images at the source position of \mathbf{y} and ρ is the angular radius of source normalized to the Einstein angle. A detailed expression for μ is given in equations (A6) of Appendix.

The contrast in the interference fringes on the observer plane depends on the size of source star in such a way that increasing the source size decreases the contrast of the interference pattern in the light curve. This effect can be seen in the Young experiment when we increase the size of the pinhole as the source in double slit experiment. The superposition of the fringes from different parts of a source in the observer plane is an indicator for the spatial coherency of the source. A mathematical criterion for losing spatial coherency is that the constructive interference from one part of source overlap with the destructive interference from the other part of the source in the observer plane.

Now we apply the spatial coherency condition of the Young experiment to the microlensing effect. Let us consider a source with size L_s located at distance of D_{ls} from the lens plane. For light rays arriving at the lens plane within a domain of radius h from the optical axis of the system, the spatial coherency condition is met if

$$L_s < \frac{D_{ls}\lambda}{2h}. \quad (19)$$

For a single lens, the angular separation between the images is given by $\Delta\theta = \sqrt{\beta^2 + 4\theta_E^2}$, where β is the impact parameter. For high-magnification events, $\Delta\theta \simeq 2\theta_E$ and the separation between the images is given by $2h = D_{ol}\Delta\theta \simeq 2D_{ol}\theta_E$. Rewriting equation (19) in terms of the source size and Einstein angle, constraint on the spatial coherency of the source is given by

$$L_s < \frac{D_{ls}}{D_{ol}} \frac{\lambda}{2\theta_E}. \quad (20)$$

λ	3 cm	1 mm
$L_s(M_\oplus)$	3.4×10^6	114
$L_s(M_J)$	2.0×10^5	6.7

Table 1. Coherent size of a source in kilometer for a single microlensing system. Here $D_s = 8.5 \text{ kpc}$, $D_l = 4 \text{ kpc}$. The observation is performed with the two wavelengths of 3cm and 1mm for the cases of earth and Jupiter mass lenses. Content of this table shows the size of coherent sources.

Using the definition of the Einstein angle, we have

$$L_s < \frac{\lambda}{2} \sqrt{\frac{D_{ls}D_s}{2R_sD_{ol}}}, \quad (21)$$

where R_s is the Schwarzschild radius of the lens. This calculation is done for a single lens. In the next section we recalculate coherency condition for a binary lens, using the Fermat potential. The advantage of a binary lens is that this lensing system can produce very close images during the caustic crossing. These images may satisfy the spatial coherency condition of the source star. Before studying the spatial coherency of a source in the binary lensing, let us estimate the coherent size of the source for a single lens.

We assume a lens at the middle of distance between the observer and source where the probability of microlensing observation is maximum (i.e. $D_{ol} = D_{ls}$). For two typical planets with masses of the Earth and Jupiter, the Schwarzschild radius is about 1 and 286 cm, respectively. For a source star at the Galactic bulge, $D_s = 8.5 \text{ kpc}$, Table (1) shows the coherent size of sources at various wavelengths. For $\lambda = 3 \text{ cm}$, we can observe the wave optics features of an earth-mass lens with a solar type source star. We can also observe the wave optics effect for a Jupiter-mass planet and a smaller source. At micron wavelengths, the spatial coherency decreases to 10 – 100 km , where we may detect diffraction pattern of smaller structures such as granules on the surface of source star. (Yu et al 2011).

As already noted, in binary lensing, during the approach of the source star to a caustic line, the distance between the pair of images can be very small compare to the case of a single lens. At the same time we may have wide images located a few astronomical units away from each other. Hence, the light rays received from the lens plane to the observer are a mixture of close coherent images and wide incoherent images. In the next section we discuss the possibility of producing a diffraction pattern by a binary lens.

3 LIGHT CURVE NEAR CAUSTIC LINE: BINARY LENSES

In this section we use numerical and semi-analytical methods to study the light curve of a microlensing event by a binary lens. During the caustic crossing, where images form at the critical lines, we can write the lens equation. In other word, the first derivatives of the Fermat potential is zero:

$$\phi_1^{(0)} = \phi_2^{(0)} = 0.$$

Diagonalizing the Fermat potential with respect to the second derivatives, we can set $\phi_{12}^{(0)} = \phi_{21}^{(0)} = 0$. In order to satisfy singular Jacobian transformation on the critical lines, from equation (6),

either ϕ_{11} or ϕ_{22} should be zero. We set $\phi_{22}^{(0)} = 0$ and $\phi_{11}^{(0)} \neq 0$. Ignoring \mathbf{x}^2 in the geometric term compare to \mathbf{y}^2 term, we perform a Taylor expansion of the Fermat potential around the critical line as (Schneider et al. 1992; Jaroszyński & Paczyński 1995):

$$\begin{aligned} \phi(\mathbf{x}, \mathbf{y}) &= \phi^{(0)} + \frac{1}{2}\mathbf{y}^2 - \mathbf{x} \cdot \mathbf{y} + \frac{1}{2}\phi_{11}^{(0)}x_1^2 + \frac{1}{6}(\phi_{222}^{(0)}x_2^3 \\ &+ \phi_{111}^{(0)}x_1^3) + \frac{1}{2}(\phi_{112}^{(0)}x_1 + \phi_{122}^{(0)}x_2)x_1x_2 + \dots \end{aligned} \quad (22)$$

Using the Fermat principle of $\delta\phi/\delta x_i = 0$, we obtain the position of the images as a function of position of the source,

$$y_1 = \phi_{11}^{(0)}x_1 + \frac{1}{2}\phi_{111}^{(0)}x_1^2 + \phi_{112}^{(0)}x_1x_2, \quad (23)$$

$$y_2 = \frac{1}{2}\phi_{222}^{(0)}x_2^2 + \phi_{122}^{(0)}x_1x_2. \quad (24)$$

Singularity for the new Jacobian of transformation implies the constrain of $\phi_{122}^{(0)}x_1 + \phi_{222}^{(0)}x_2 = 0$, where we have ignored the higher order terms of x ,

From equations (23) and (24), we obtain the position of the images as follows:

$$\mathbf{x}_{images} = \left(\frac{y_1}{\phi_{11}^{(0)}}, \pm \sqrt{\frac{2y_2}{\phi_{222}^{(0)}}} \right), \quad (25)$$

where y_1 is chosen along the caustic line and y_2 is perpendicular to the caustic line. On the positive side of y_2 we have two images while for the negative side there is no image. Substituting the position of the images in equation (22), we can calculate the Fermat potential for the nearby images during the caustic crossing. The difference between the Fermat potentials of the two images is given by

$$\Delta\phi = \frac{2}{3} \frac{(2y_2)^{\frac{3}{2}}}{(\phi_{222}^{(0)})^{\frac{1}{2}}}. \quad (26)$$

Here $\Delta\phi$ is a function of y_2 and the third derivative of Fermat potential on the critical line. Assuming the trajectory of the source (i.e. $\vec{y}(t)$) has a direction given by the angle γ with respect to the caustic line, the position of the source in the direction perpendicular to the caustic line is given by $y_2 = \sin \gamma \times (t - t_c)/t_E$. On the other hand, from the Fermat potential for a binary system in equation (16), we can calculate $\phi_{222}^{(cm)}$ in the center of mass coordinate system as follows:

$$\begin{aligned} \phi_{222}^{(cm)} &= m_p \left[\frac{6x_2}{((x_1 - x_{p1})^2 + x_2^2)^2} - \frac{8x_2^3}{((x_1 - x_{p1})^2 + x_2^2)^3} \right] \\ &+ m_* \left[\frac{6x_2}{((x_1 - x_{*1})^2 + x_2^2)^2} - \frac{8x_2^3}{((x_1 - x_{*1})^2 + x_2^2)^3} \right]. \end{aligned} \quad (27)$$

Here x_1 and x_2 represent the position of the critical lines on which images form during the caustic crossing. The position of images on the critical line depends on the location of the source, and double images can form along the critical line, either around the star (wide images) or around the planet (close images). These pairs of images split from single image during the caustic crossing. Because our calculation has been done on the local coordinates of the critical line where images form, we perform a coordinate transformation of the Fermat potential from the center of mass coordinate system to the local diagonalized coordinate system at the image position. First we do a boost along the x-axis to one of lens positions. The second boost is along the radial direction, equal to the Einstein radius of lens. Finally, we perform a rotation with R_{ij}

to diagonalize ϕ_{ij} . The third derivative of the Fermat potential which is the relevant parameter in the Fermat potential in equation (26) can be obtained after the coordinate transformation as follows $\phi_{222}^{(0)} = R_{2i}R_{2j}R_{2k}\phi_{ijk}^{(cm)}$.

The corresponding coordinate transformations to the location of images around the critical line of the planet is given by $x_1 = x_{p1} + R_E^{(p)}/R_E \cos \theta$ and $x_2 = R_E^{(p)}/R_E \sin \theta$ where $R_E^{(p)}$ is the Einstein radius of the planet, R_E is the overall Einstein radius and θ is the polar angle with respect to the line connecting the two lenses. Since $|R_{ij}| \sim 1$, the magnitude of the third order derivative of the Fermat potential doesn't change so much by the coordinate transformation, $\phi_{222}^{(0)} \simeq \phi_{ijk}^{(cm)}$. Substituting boosts in equation (28), since $m_* \gg m_p$, the first term dominates as $R_E^{(p)}$ appears in the denominator, and hence

$$\phi_{222}^{(0)} \simeq -m_p \left(\frac{R_E^{(p)}}{R_E} \right)^{-3}. \quad (28)$$

Replacing the ratio of Einstein radius of the planet to the Einstein radius of the star with the corresponding mass ratio and using a normalized planet mass with $m_p = q/(1+q)$, equation (28) can be written as

$$\phi_{222}^{(0)} \simeq -\frac{1}{\sqrt{q}}. \quad (29)$$

Comparing the images that form around the planet and the parent star on the lens plane, the nearby images around the planet are more suitable for producing a diffraction pattern on the observer plane. Having a smaller q results in a larger $\phi_{222}^{(0)}$ and consequently a smaller $\Delta\phi$. We now substitute equation (29) into equation (26) and replace the difference in the Fermat potential with the difference in the time delay between the trajectory of the two images as follows:

$$\begin{aligned} \Delta t &= 2 \times R_s \Delta\phi \\ &= 5 \times 10^{-9} \\ &\times \left(\frac{t - t_c}{1h} \sin \gamma \right)^{3/2} \left(\frac{t_E}{40days} \right)^{-3/2} \left(\frac{q}{0.001} \right)^{1/4} \left(\frac{M}{M_\odot} \right) sec \end{aligned}$$

where $(t - t_c)/1h$ is the time corresponds to the relative distance of the source from the caustic line which is normalized to one hour. We note that, unlike for the single lens where Δt is of the order of light crossing time of the Schwarzschild radius, in the case of a binary lens the factor q decreases the corresponding time-scale (Heyl 2010). On the other hand, as $t \rightarrow t_c$, Δt approaches zero. The characteristic time difference in the Fermat potential is about $\Delta t \sim 5 \times 10^{-9} s$ corresponding to $\Delta l \sim 150 cm$. This length scale corresponds to the frequency of 0.2 GHz. Here wavelengths larger than this threshold Δl satisfy temporal coherency and can produce a diffraction pattern from the images on the observer plane. Repeating this calculation for the distant images on the lens plane, where q is of the order of one, we obtain a larger value for Δt , destructive for producing the wave optics features. We note that wavelength $\lambda \sim 150 cm$ is a typical size of wavelength for temporal coherency and near the caustic crossing as Δl approaches zero, we can observe a diffraction pattern in the shorter wavelengths.

The other essential condition to have wave optics feature, as discussed in the previous section, is the spatial coherency of the source. From equation (25), the physical distance between the images on the lens plane, rewriting the dimensionless parameter of x_{image} in terms of the Einstein radius, is given by

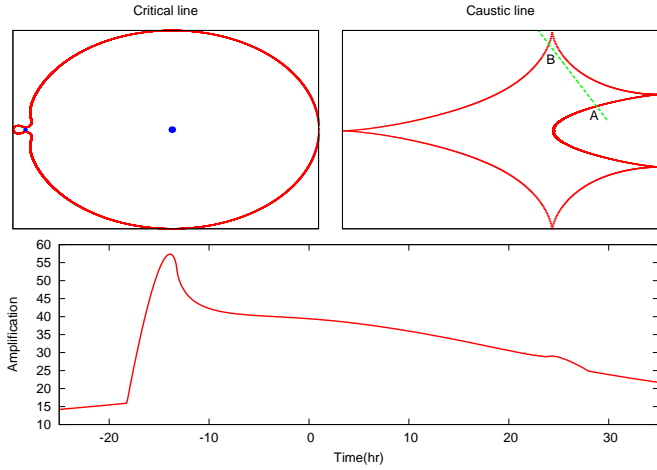


Figure 3. Critical lines (top left panel), caustic lines (top right panel) and light curve in the geometric optics (lower panel) for a binary system with the parameters of $q = 0.001$, $d = 1$. Here we take source star with the size of $\rho = 0.002$. Large loop (at the top left panel) corresponds to the critical line of the parent star lens and smaller loop corresponds to the critical line of the planet. The straight dashed line (at the top right panel) indicates the path of the source on the source plane.

$$h = 2R_E \sqrt{\frac{2y_2}{\phi_{222}^{(0)}}}. \quad (30)$$

Substituting h in equation (19) and expressing y_2 in terms of transit time, the condition of spatial coherency for a binary lens system is given as follows:

$$L_s < \frac{\lambda D_{ls}}{4R_E} \sqrt{\frac{t_E \phi_{222}^{(0)}}{2(t - t_c) \sin \gamma}}, \quad (31)$$

and we can rewrite this equation in terms of characteristic scales of the lens and source as follows:

$$L_s < 1.59 \times 10^6 \left(\frac{\lambda}{10\text{cm}}\right) \left(\frac{D_{ls}}{4\text{kpc}}\right) \left(\frac{R_E}{1\text{a.u.}}\right)^{-1} \times \left(\frac{t_E}{40\text{days}}\right)^{0.5} \left(\frac{q}{0.001}\right)^{-0.25} \left(\frac{t - t_c}{10\text{hr}}\right)^{-0.5} \text{ km}. \quad (32)$$

Note that L_s on the left-hand side of this inequality represents the part of the source that crosses the caustic line. Here, only this part of source contributes in production of close-pair images. Hence even for larger sources, we may have spatial coherency condition at the beginning of the caustic crossing.

The other observable parameter which depends on the position of source and relative motion with respect to the caustic lines is the magnification. Substituting equation (22) into equation (7) and keeping the leading terms in the Fermat potential, the magnification near the caustic is obtained as follows (Schneider et al. 1992):

$$\mu \sim [Ai(\frac{y_2}{Y_0})]^2, \quad (33)$$

where $Y_0 = (\frac{|\phi_{222}|}{2f^2})^{1/3} \sim q^{-1/6}$ and $Ai(x)$ is the Airy function. The maximum magnification also relates to the derivatives of the Fermat potential via $\mu_{max} \propto |\phi_{11}^{(0)}|^{-1} |\phi_{222}^{(0)}|^{-2/3} \sim q^{1/3}$. Near the critical line for the close-images, larger $\phi_{222}^{(0)}$ gives a smaller maximum magnification for the fringes in the light curve and larger Y_0 produces longer modes. On the other hand, for the wide im-

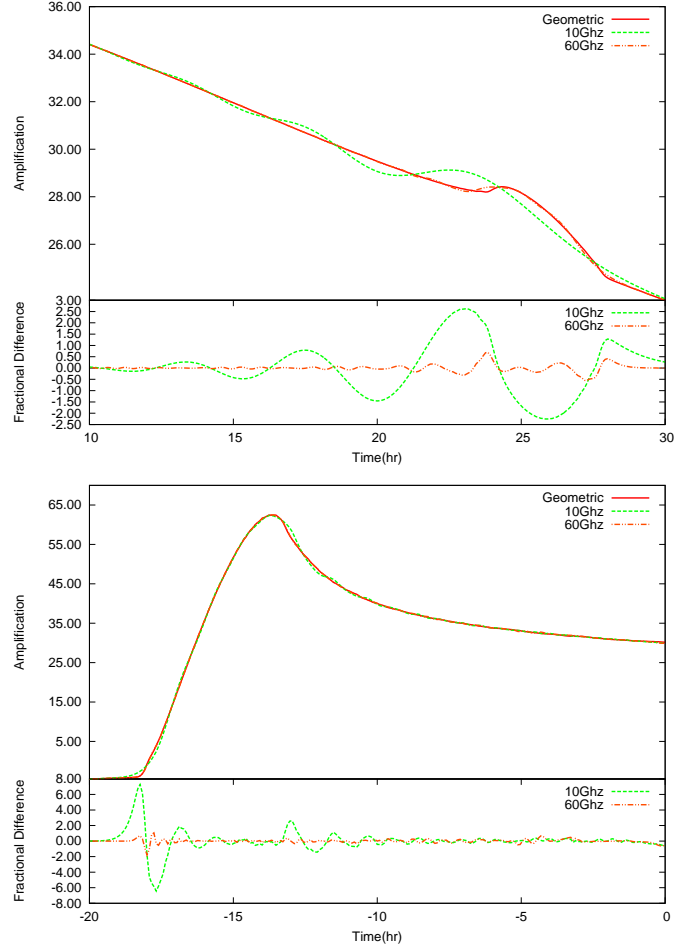


Figure 4. The light curves correspond to the close pair images (upper panel) around the planet and wide pair images (lower panel) around the parent star in a binary lenses. Here the source crosses the caustic line at points A and B (shown in Figure 3). The solid line corresponds to the geometric optics and two wave optics light curves are shown in 10 GHz (dashed line) and 60 GHz (dashed-dotted line). The smaller panels in each figure correspond to the fractional difference (in percentage) between the geometric optics and the wave optics.

ages around the lens star, q is large, $\phi_{222}^{(0)}$ is small and we have shorter modes of the diffraction pattern with larger magnification (i.e. closer to the geometric optics case). We recall that in the diagonalized coordinate system for the Fermat potential, ϕ_{11} is the non-zero term of the second-order derivative of the Fermat potential. On the other hand, the trace of ϕ_{ij} is $\nabla^2 \phi = 2 - \nabla^2 \psi$, where for two point-mass lenses the second term on the right-hand side of this equation is the Dirac delta function at the position of the lenses. We can set this function to zero along the caustic lines, far from the position of the lenses. Hence for a small distance from the caustic lines, $\phi_{11} = 2$. Therefore, the only relevant parameters in the wave optics light curve are f , ϕ_{222} and trajectory of the source with respect to the caustic line.

Fig. (3) shows the configuration of a binary lens (parent star and planet) with the corresponding critical and caustic lines and the light curve for geometric optics. Caustic crossing takes place at points A and B , producing close and wide images. Fig. (4) also compares the light curves in the wave optics and geometric optics

formalisms for two wavelengths at points A and B . The light curves are obtained from the Fresnel-Kirchhoff integration. For the close images, the time variation of the fringes is slower than for the wide images. This effect can be seen from the relative velocity between the separation of the pair images from equation (30) as follows:

$$\dot{h} = v_t \sqrt{\frac{2t_E}{|t - t_c|} \times \frac{\sin \gamma}{\phi_{222}^{(0)}}}, \quad (34)$$

where $v_t = R_E/t_E$ is the relative velocity of the source with respect to the lens. For the close-pair images, we have a larger $\phi_{222}^{(0)}$ and for the wide-pair images this term is smaller. Hence not only close-images produce large modes of fringes, their time variation also slower and provides enough time for the observer to detect this effect with a suitable cadence of observations.

4 OBSERVATIONAL PROSPECT

In this section we study the possibility of follow-up observations of a binary microlensing system during the caustic crossing by the future SKA project. For a single lens, the parameters involved in the light curve are the Einstein crossing time t_E , the minimum impact parameter u_0 and the time for the maximum magnification t_0 . Amongst these parameters, the only parameter that contains the physical information of the system is t_E which is a function of the mass of lens, the relative distance of the lens with respect to the source and observer and the transverse velocity of the lens with respect to our line of sight. Using additional information such as the parallax effect due to the annual motion of the earth around the Sun (Gould 1998), one can partially break the degeneracy between the lens parameters (Rahvar et al. 2003). However, the finite-size effect of the source can also provide extra information to break the degeneracy between the lens parameters (Roulet & Mollerach 1997).

Increasing the number of lenses from one to two increases the number of parameters of the lensing system. The additional parameters are (i) the projected distance between the lenses normalized to the Einstein radius, " d ", (ii) the relative mass of the lenses, " q " and (iii) the angle " α " defining the trajectory of the source with respect to the line joining the two lenses. For a binary system, we have a total of six parameters to fit the light curve. The probability of microlensing observation of a binary lens depends on the size of the caustic and for the case of resonance where the distance between the lenses is of the order of Einstein ring, we will have the maximum probability of detection.

The main problem with the resonance events is that, in spite of occasional observations of planets, owing to our lack of our knowledge about observational efficiency, it is difficult to analysis the distribution function of the parameters of the planet. There have been some efforts to develop a fully deterministic strategy through automated searching system for exoplanets (Dominik et al 2010). Having such a system to cover all the known microlensing candidates will enable us to obtain a correct statistical distribution of the parameters of the planet. The other important channel for exoplanet observation is that of high-magnification events (Griest & Safizadeh 1998). Almost all the very high magnification events can be flagged by microlensing surveys and follow-up telescopes monitor them with a high sampling rate and better photometric precision. Unlike the case for low-magnification events, for these events, the detection efficiency function is almost known and statistical analysis in the parameter space can be applied (Gould et al. 2010). One of the main problems with the binary

lenses is the $d \leftrightarrow d^{-1}$ degeneracy problem, whereby we can have almost the same light curve for the close and wide binary lenses.

In the caustic classification of the binary systems we have three type of topologies for the caustics and corresponding critical lines (Schneider & Weiß 1986), the so-called the "close", "wide" and "intermediate" or resonance binaries. Fig. (5) shows these three categories of caustic lines for three values of planet to the star mass ratios. To study the wave optics feature during the caustic crossing, we generate synthetic light curves for the three categories and compare the results with the geometric optics features. Our aim is to study the wave optics signals in the resonance and high-magnification channels.

In order to quantify the wave optics feature in the light curve, we use the χ^2 difference from the best fit of the wave optics and geometric optics. Assuming σ_i as the error bar for each data point, $\mu_i^{(g)}$ as the magnification in the geometric optics and $\mu_i^{(w)}$ as the magnification in the wave optics, the difference between the χ^2 s is given by

$$\begin{aligned} \Delta\chi^2 &= \chi_g^2 - \chi_w^2 \\ &= \sum_{i=1}^N \frac{1}{\sigma_i^2} (\mu_i^{(w)} - \mu_i^{(g)}) (2\mu_i^{(exp)} - \mu_i^{(w)} - \mu_i^{(g)}). \end{aligned} \quad (35)$$

Having a threshold for $\Delta\chi^2$, we can distinguish the wave optics light curve from the for the geometric optics. An important element in equation (35) is the estimation of the photometric error which depends on the source flux, integration time and the size of the radio telescope. Amongst the various sources, red giants and super-giants can emit electromagnetic waves at longer wavelengths. Radio-loud Quasars at the cosmological scales are also bright radio sources.

Detailed studies on radio sources are performed for single-lens wave optics microlensing in (Heyl 2011). In what follows we adapt that classification. For the red giants, a closer star such as Arcturus (Perryman et al. 1997) emits at the wavelengths of 2cm and 6cm with 0.68 mJy and 0.28 mJy, respectively (Drake & Linsky 1986). The spectrum of this type of star is given by

$$f_\nu \simeq 24 \left(\frac{\nu}{GHz}\right)^{0.8} \left(\frac{kpc}{D_s}\right)^2 \text{ nJy}. \quad (36)$$

Another class is that of low-mass late-type stars as asymptotic giants. For example, Mira is an example of this class and its spectrum is given by (Perryman et al. 1997; Reid et al. 1997)

$$f_\nu \simeq 72 \left(\frac{\nu}{GHz}\right)^2 \left(\frac{kpc}{D_s}\right)^2 \text{ nJy}. \quad (37)$$

Finally super-giants have strong radio emission. Betelgeuse is a red super giants located at a distance of 197 pc (Newell & Hjellming 1982; Harper et al. 2008). The spectrum of this star normalized to the kiloparsec distance is

$$f_\nu \simeq 9.3 \left(\frac{\nu}{GHz}\right)^{1.32} \left(\frac{kpc}{D_s}\right)^2 \mu\text{Jy}. \quad (38)$$

The radii of super-giants are of the order of a few astronomical unit. Assuming these stars are in the Galactic center at $\sim 8kpc$ distance from us, from equation (32), we can obtain coherent images for close-images on the lens plane. As mentioned above, at the caustic crossing, only a small part of the source contributes to the production of coherent close-pair images.

In equation (35), we need an estimation for the photometric error bar. For the SKA project the noise corresponds to Nyquist sampling is 0.27 Jy (Schilizzi et al. 2007). This sampling is defined such that the integration time multiplied by the band width, is equal to one (i.e. $\Delta\nu \Delta\tau = 1$). Because noise decreases with the square

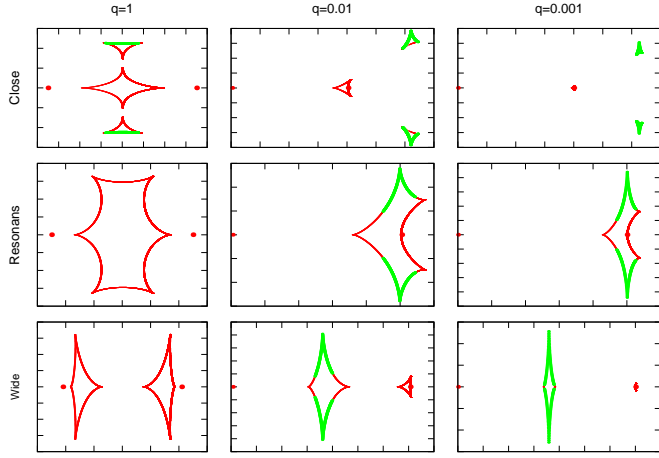


Figure 5. Caustic lines for three categories of wide, close and intermediate separation of two lenses with three different values of q . The classification for the separation of the lenses is based on three topology of the caustic lines (Schneider & Weiß 1986). The thick-green lines of the caustic produces light curves with $\Delta\chi^2 > 5$ in equation (35). The binary lenses are indicated by two spots and scales in the figures are given in terms of distance between the lenses.

root of time and the band width as $1/\sqrt{\Delta\nu\Delta\tau}$, we can write the noise in terms of these two parameters as follows:

$$\Delta f = 0.14 \left(\frac{\Delta\nu}{\text{GHz}} \right)^{-1/2} \left(\frac{\Delta\tau}{1\text{hr}} \right)^{-1/2} \mu\text{Jy}. \quad (39)$$

We use the six parameters of the binary microlensing system to simulate the light curves. Also the source star is assumed to radiate at longer wavelengths. We compare the simulated data in the geometric optics case with the wave optics case and use the criterion of $\Delta\chi^2 > 5$ between the two theoretical light curves. For an ensemble of light curves, we identify caustic lines in three categories of binaries, as shown in Fig. (5). Those light curves with caustic crossing satisfy the criterion for the wave optics are identified in the figure. Our analysis shows that wave optics feature is sensitive to the specific parts of the caustic lines of a binary lens.

As we noted before, there are two main channels for the exoplanet observations. In Figure (5) we identify area of caustic lines in each channel with the wave optics feature. Having a small q , wide and close binaries can produce almost the same geometric optics light curves. According to Figure (5), there is no strong wave optics effect in the light curve of the high magnification events. On the other hand for the intermediate regime (resonance) a larger area of the caustic lines is suitable for the wave optics effect. In this case, we will have a combination of close and wide images on the lens plane.

We perform a Monte-Carlo simulation to generate an ensemble of light curves and study the wave optics effect in the simulated light curves. Fig. (6) shows a sample of light curve in this simulation with the cadence rate of 45 min and signal-to-noise ratio of $S/N = 7$. The relevant parameters of the wave optics from equation (33) are the wavelength in the Airy function, Y_0 and the maximum magnification of the light curve, μ_{max} . These parameters depend on f and ϕ_{222} . For an ensemble of light curves distributed uniformly in parameter space, we calculate the χ^2 difference between the wave optics and the geometric optics from equation (35). In order to study the sensitivity of discriminating param-

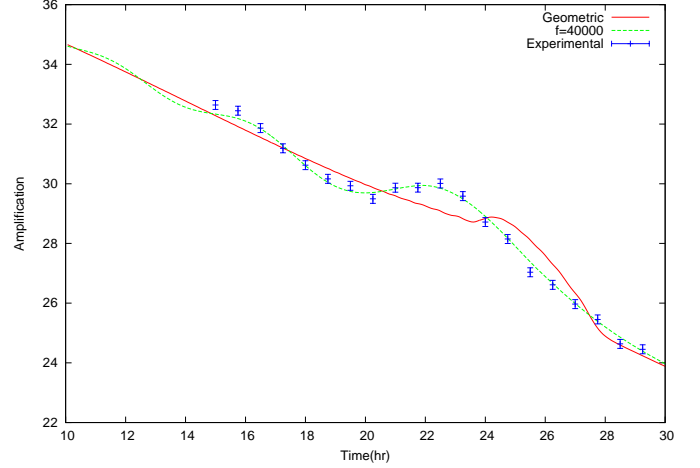


Figure 6. Simulation of the microlensing light curve in a binary lens. The parameters of the lens is taken as the light curve in Figure (3). The data points are simulated according to the noise in SKA. Here we have a signal-to-noise of 7 with 45 minute integration time. The observation is done in 10 GHz. The solid line represents the best fit in the geometric optics and the dashed line represents the best fit of the light curve including the the wave optics effect.

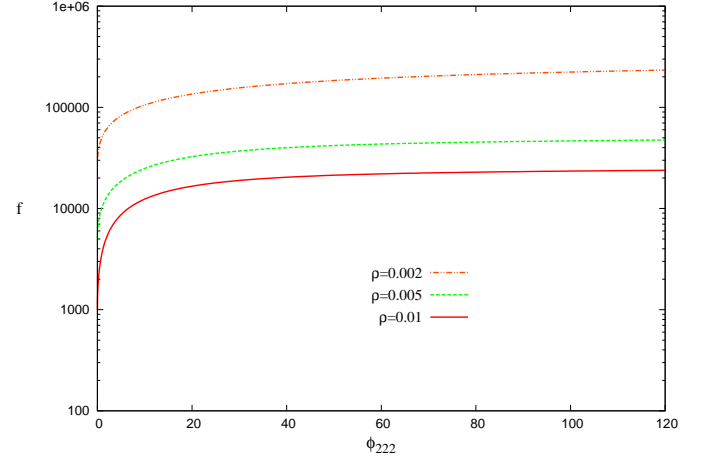


Figure 7. Wave optics features are excluded in the area above the curves in the parameter space of f and ϕ_{222} according to criterion $\Delta\chi^2 > 10$. The size of the source star normalized to the Einstein radius is mentioned in the legend of Figure. Smaller stars are favorable for the observation of the wave optics features in microlensing.

eter, $\Delta\chi^2$, in terms of f and ϕ_{222} , we identify area of parameter space that satisfies $\Delta\chi^2 > 10$ where the source sizes are chosen $\rho = 0.001, 0.005$ and 0.002 , see Fig. (7). Here the upper part of these curves do not satisfy our criterion and are excluded. Having smaller f means longer wavelength for the observation. On the other hand, ϕ_{222} relates to the maximum magnification and size of modes from the wave optics. By measuring how the transit time-scale of the fringes changes with respect to the observer $\Delta\tau$, we can determine $Y_0(f, \phi_{222}^{(0)}) = \Delta\tau/t_E$. However, $\mu_{max}(\phi_{222})$ can be measured directly from the light curve.

The physical parameters involved in the wave optics light

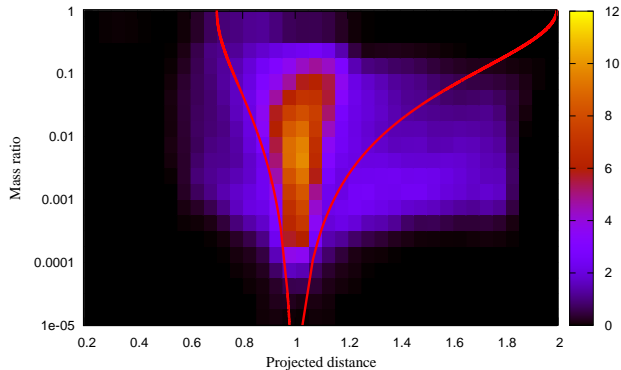


Figure 8. Efficiency function in terms of d and q , comparing the wave optics features with the geometric optics. The criterion for the wave optics light curve from equation (35) is $\Delta\chi^2 > 10$. The simulation is done for the source star with the finite size of $\rho = 0.005$ and observation at $\nu = 10\text{GHz}$. The six parameters of the lens are generated with the uniform distribution. Red lines separate the parameter space according to the definition of the wide, close and intermediate binaries (Erdl & Schneider 1993).

curves are the overall mass of system M_t , the mass ratio q and trajectory of the source with respect to the lens. In contrast, from observations in the geometric optics case, we can find six parameters of the light curve with a degree of degeneracy. Having extra information from the wave optics will constrain M_t and q parameters and subsequently we can identify the parameters of planet with better accuracy.

We now want to look at the sensitivity of the wave optics signals in terms of the physical parameters of the binary system, q and d . From the Monte-Carlo simulation, we select a fraction of events that satisfy the condition $\Delta\chi^2 > 10$. According to Fig. (8), a suitable area of the parameter space for the wave optics features is in the resonance area where the separation between the lens and the planet is of the order of Einstein radius. This result is compatible with our preliminary analysis for the sensitivity of wave optics signal in terms of the parameter space in Fig. (5). In order to estimate the overall number of microlensing events with the wave optics signals, we should multiply the efficiency function with the real distribution of binary lenses in terms of q and d .

Finally, we want to extract physical information from a typical wave optics light curve, assuming that we have observational data at both visual and radio wavelengths. From the data of geometric optics, by fitting to the light curve we can extract q , d and the trajectory of the source. On the other hand, from the wave optics our relevant variables are f and $\phi_{222} \sim 1/\sqrt{q}$. Measurement of these two parameters provides directly the value of q and the overall mass of the lenses. Assuming a set of simulated data points of the light curve, let us extract the observable parameters from this light curve. We fit the simulated data in Fig. (9) with the theoretical wave optics light curve. Here the theoretical value of f is 49475, assuming that observations are performed at $\nu = 10\text{GHz}$, and from the likelihood function we obtain $f = 51400^{+1635}_{-1600}$. Using k from the definition of f , we can extract the overall mass of a binary system. We can also extract the mass ratio of the planet to the parent star from the wave optics light curve.

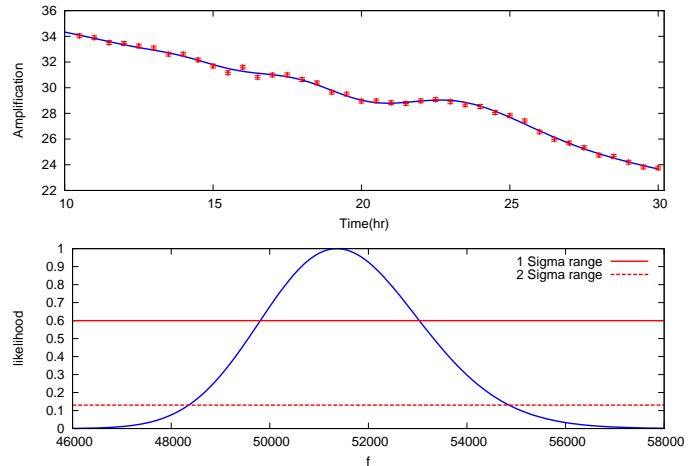


Figure 9. The synthetic light curve in the radio wave lengths is generated with the cadence of 30 min and error bar of 0.15 and fitted with the wave optics theoretical light curve. The initial value of f is taken 49475. We use $\nu = 10\text{GHz}$ in the simulated light curve for the observation. The likelihood function shows the best fit with 1σ and 2σ level of confidences. For 1σ , we have $f = 51400^{+1635}_{-1600}$, provides 6% uncertainty in mass measurement.

5 CONCLUSION

In this work we studied the wave optics effect of gravitational microlensing by a binary lens composed of a lens star and a companion planet. The lensing effect of a planet during the caustic crossing produces close images, a suitable configuration for the images on the lens plane to generate diffraction pattern on the observer plane. This effect is an example of Young's double-slit experiment in the astronomical scales. We derived the wave optics features of a binary lens, showing that it depends only on the third-order derivatives of the Fermat potential ϕ_{222} and $f = 2kR_s$.

We take red giants and super-giants as the source stars of gravitational microlensing toward the Galactic bulge, as there is a natural selection bias for observing this type of source stars. We suggested using SKA future project for the observation of the wave optics signals in the light curve. In this observational program, radio observatories accompany the microlensing follow-up telescopes in the visual bands. These two observations at long and short wave lengths can provide a complimentary program for studying binary microlensing events to break the degeneracy of binary systems. We discussed the problem of spatial coherency of sources in binary lensing and showed that only the part of the source that crosses the caustic line contributes to the formation of close-pair images. While an extended giant star may have no spatial coherency, the spatial coherency condition holds for the small part of the source crossing the caustic line.

We studied the observability of the wave optics parameters in a Monte Carlo simulation by fitting the simulated microlensing light curves with the theoretical wave optics light curve. Out of the two channels for the detection of exoplanets by microlensing, namely (i) the high-magnification channel and (ii) the resonance channel, we showed that the wave optics observation is in favour of resonance binary microlensing events. The extra information from the wave optics light curve enable us to solve for the lens parameters with better accuracy. Our analysis has shown that the use of radio tele-

scopes for observations of planetary microlensing events will open a new window for studies of exoplanet .

ACKNOWLEDGMENTS

AM thanks Sharif university of Technology providing high performance computational facilities. We thank Avery Broderick, Vahid Karimipour and Mir Abbas Jalali for providing useful comments and improving text of paper. We also would like to thank anonymous referee for valuable comments. This research was supported by Perimeter Institute for Theoretical Physics and the John Templeton Foundation. Research at Perimeter Institute was supported by the Government of Canada through Industry Canada and by the Province of Ontario through the Ministry of Economic Development and Innovation.

REFERENCES

- Arnold, V. I., 1989, *Mathematical Methods of Classical Mechanics*, 2nd edition, Springer-Verlag, New York.
- Born, M., Wolf, E., *Principles of Optics*, Cambridge University Press. 7th edition, 2002.
- Dominik M., 2007, MNRAS, 377, 1679
- Dominik, M., Jørgensen, U. G., Rattenbury, N. J., et al., 2010, *Astronomische Nachrichten*, 331, 671
- Drake S. A., Linsky J. L., 1986, *Astron. J.*, 91, 602
- Erdl, H., & Schneider, P. 1993, *A&A*, 268, 453
- Einstein A., 1936, *Science*, 84, 506
- Gould, A., 1998, *ApJ*, 506, 253
- Gould, A., Dong, S., Gaudi, B. S., et al., 2010, *ApJ*, 720, 1073
- Griest, K., & Safizadeh, N., 1998, *ApJ*, 500, 37
- Guenther, B. D., 1990, *Modern Optics*, John Wiley and Sons, Inc.
- Hamadache, C. et al., 2006, *A&A*, 454, 185
- Harper, G. M., Brown A., Guinan, E. F., 2008, *Astron. J.*, 135, 1430
- Heyl, J. S., 2010, MNRAS, 402, L39
- Heyl, J. S., 2011, MNRAS, 411, 1780
- Heyl, J. S., 2011, MNRAS, 411, 1787
- Jaroszyski, M., Paczyński B., 1995, *ApJ*, 455, 443
- Mandzhos, A. A., 1981, *Pis'ma Astron. Zh.*, 7, 387
- Mao, S., Paczyński, B., 1991, *ApJ*, 374, L37.
- Mehta, C., 1963, *Nuovo Cimento*, 28, 401
- Messineo, M., Habing, H. J., Menten, K. M., Omont, A., Sjouwerman, L. O., Bertoldi, F., 2005, *A&A*, 435, 575
- Moniez, M., Rahvar, S., Ansari, R., Perdereau, O., in preparation.
- Newell, R. T., Hjellming, R. M., 1982, *Astrophys. J Lett*, 263, L85
- Ohanian, H. C., 1983, *ApJ*, 271, 551
- Paczyński, B., 1986, *ApJ*, 304, 1
- Perryman, M. A. C., et al., 1997, *Astron. Astrophys.*, 323, L49
- Rahal, Y. R., Afonso, C., Albert, J.-N., et al. 2009, *A&A*, 500, 1027
- Rahvar, S., Moniez, M., Ansari, R., & Perdereau, O., 2003, *A&A*, 412, 81
- Reid, M. J., Menten, K. M., 1997, *ApJ*, 476, 327
- Roulet, E., & Mollerach, S., 1997, *Physics Report*, 279, 67
- Schilizzi, R. T., et al., 2007, *Antennas and Propagation Society International Symposium 2006, IEEE*, 9-14
- Schneider, P., Weiβ, A., 1986, *A&A*, 164, 237
- Schneider, P., & Schmid-Burgk, J., 1985, *A&A*, 148, 369

- Schneider, P., Ehlers, J., Falco, E. E., 1992, *Gravitational Lenses*, Springer-Verlag, Berlin
- Vlemmings, W. H. T., van Langevelde, H. J., Diamond, P. J., 2005, *Memorie della Societ Astronomica Italiana*, 76, 462
- Walsh, D., Carswell, R. F., Weymann, R. J., 1979, *Nature*, 279, 381
- Daren, Y., Zongxia, X., Qinghua, H., Shuhong, Y., Jun, Z., Jingxiu, W., 2011, *ApJ*, 743, 58
- Zabel, S. A., Peterson, J. B., 2003, *The Astrophysical Journal*, 594, 456

APPENDIX A: COHERENCY IN WAVE OPTICS: GRAVITATIONAL LENSING

In this appendix we adapt the wave optics notations used in Schneider et al. (1992). Starting from the amplitude of electromagnetic waves on the lens plane, we can obtain the amplitude on the observer plane from the superposition principle as

$$V = \int e^{if\phi(x,y)} d^2x. \quad (A1)$$

We perform a Taylor expansion of the Fermat potential around images and diagonalize the second-order derivatives of the potential. The amplitude of the electromagnetic waves on the observer plane is

$$V = \int e^{if[\phi^{(0)} + \frac{1}{2}(\phi_{11}^{(0)}x_1^2 + \phi_{22}^{(0)}x_2^2)]} d^2x. \quad (A2)$$

Integrating from equation (A2), we find

$$V = \frac{2\pi i}{f} \frac{1}{\sqrt{\det |J|}} e^{if(\phi^{(0)} - n_i\pi/2)}, \quad (A3)$$

where $\det |J|$ is the determinant of $\phi_{ij}^{(0)}$, which is given in equation (6). Here n refers to the type of images and can be equal to $n = 0, 1, 2$, depending on the number of focal points transverse from the source to the observer (Arnold 1989). Now if we have N images from the lensing, the overall amplitude is given by

$$V = \frac{2\pi i}{f} \sum_{i=1}^N \frac{e^{i(f\phi_i^{(0)} - n_i\pi/2)}}{\sqrt{|\det J_i|}}. \quad (A4)$$

We note that this equation is valid while the source is out of the caustic lines (i.e. $\det |J_i| \neq 0$). We assume a spectrum for the source and replace f with $2\omega R_s$, the overall amplitude can be written as

$$V = 2\pi i \sum_{i=1}^N \frac{1}{\sqrt{|\det J_i|}} \int \frac{1}{f(\omega)} e^{i(2R_s\omega\phi_i^{(0)} - n_i\pi/2)} g(\omega) d\omega. \quad (A5)$$

Finally, the overall magnification obtain from $\mu = VV^*$. After averaging over time, the magnification is given by

$$\begin{aligned} \mu &= \sum_{i=1}^N \mu_i \\ &+ \sum_{i \neq j} \frac{4\pi^2}{\sqrt{|\det J_i| |\det J_j|}} \int \frac{g(\omega)^2}{f(\omega)^2} e^{i[f(\omega)(\phi_i^{(0)} - \phi_j^{(0)}) - \frac{\pi}{2}(n_i - n_j)]} d\omega. \end{aligned} \quad (A6)$$

Here, time integration is done over the oscillating terms of $e^{i\omega t}$ and for the cross terms the result of integration is a Dirac-Delta function. The phase term of $f(\omega)(\phi_1^{(0)} - \phi_2^{(0)})$ in the integrand depends on the phase difference between the i th and j th sources. For the

case that this phase is larger than the coherent time of the source, the result of this integral is zero and only the first term of equation (A6) is non-zero, representing the geometric optics contribute to the magnification. For the simple case of two images, $N = 2$, let us assume a Gaussian spectrum for $g(\omega)$ with a width given by $\Delta\omega$, the magnification for this simple case obtain as follows:

$$\mu = \mu_1 + \mu_2 + 2e^{-\left(\frac{\Delta t}{\tau}\right)^2} \sqrt{\mu_1 \mu_2} \cos\left[\omega_0 \Delta t - \frac{\pi}{2}(n_1 - n_2)\right], \quad (\text{A7})$$

where we replaced the width of the spectrum with the coherent time as $\Delta\omega = \frac{1}{\tau}$. For $\Delta t \ll \tau$, we have an oscillating mode that reveals the wave optics feature from the superposition of the waves. In contrast, for $\Delta t \gg \tau$ the exponential suppresses the oscillating term and we will have a geometric term for the magnification.

Now let us consider an extended source, in which each incoherent point on the source contributes to the amplitude of the electromagnetic waves on the observer plane. Hence for this case we can write equation (A5) for each point of the source, assigning it by $V(s)$. The overall amplitude can be written as

$$|V|^2 = \frac{4\pi^2}{S^2} \int \int \sum_{i,j=1}^N \frac{ds ds'}{\sqrt{|\det J_i(s)| |\det J_j(s')|}} \times \quad (\text{A8})$$

$$\int \int \frac{\langle g(\omega)g(\omega') \rangle}{f(\omega)f(\omega')} e^{i[2R_s(\omega\phi_i^{(0)}(s) - \omega'\phi_j^{(0)}(s')) - (n_i - n_j)\pi/2]} d\omega d\omega',$$

where S is the area of the source and averaging is performed over time, hence $\langle g(\omega)g(\omega') \rangle = g(\omega)^2 \delta(\omega - \omega')$. Because the differential elements on the source are spatially uncorrelated, the cross terms in equation (A8) will cancel, and only light rays propagating from the individual elements of the source contribute in this summation. Mathematically we can write

$$\langle \phi_i^{(0)}(s)\phi_j^{(0)}(s') \rangle \sim \delta(s - s').$$

Hence equation (A8) simplifies to

$$\mu = \frac{1}{S} \int ds \int \frac{g(\omega)^2}{f(\omega)^2} \sum_{i,j=1}^N \frac{e^{i[f(\omega)(\phi_i^{(0)}(s) - \phi_j^{(0)}(s)) - (n_i - n_j)\pi/2]}}{\sqrt{|\det J_i(s)| |\det J_j(s)|}} d\omega; \quad (\text{A9})$$

or, in other words, the overall magnification can be written as

$$\mu = \frac{1}{S} \int \mu(s) ds. \quad (\text{A10})$$